TENSILE STRENGTH AND FAILURE MODES OF CONTINUOUS CARBON NANOTUBE YARNS FOR STRUCTURAL COMPOSITE APPLICATION

Yourri-Samuel Dessureault, Claire Jolowsky, Samantha Bell, Stefan Spiric, Josiah Molyneux, Dr. Jin Gyu Park, Dr. Ayou Hao, Dr. Zhiyong Liang
High-Performance Materials Institute, Department of Industrial & Manufacturing Engineering, Florida A&M University – Florida State University College of Engineering
Tallahassee, FL 32310, USA

ABSTRACT

Carbon nanotubes (CNT) have shown very attractive mechanical properties. Recently, CNT yarns (CNTy) have become commercially available and are becoming a promising choice for composite structures. To gain a fundamental understanding of CNTy mechanical performance, three variations of CNTy were tested at long gauge lengths (100 – 120 mm). The as-received CNTy demonstrated the highest specific tensile strength (0.911 ± 0.137 N/tex), while the CNTy modified to maximize CNT packing showed the lowest specific tensile strength (0.337 ± 0.217 N/tex). The results were the fit to 2-parameter Weibull distributions with near 0.99 goodness of fit. This revealed that long-range CNT alignment acted as the key contributor to the tensile strength, while defects influenced the failure mode. The distribution analysis at a 95 % confidence interval of the CNTy tensile properties were conducted for potential engineering applications.

Corresponding author: Yourri-Samuel Dessureault

1. INTRODUCTION

High-performance composites have been a boon to the development of advanced aerospace systems, which currently rely on high-strength fibers, such as carbon fibers. However, improvements to these fiber systems are becoming ever increasingly difficult to achieve. Meanwhile, carbon nanotubes (CNTs) and CNT fibers provide a potential route for the evolution of fiber reinforcements due to their mechanical and multifunctional properties [1,2]. As such, CNTs have been studied since Iijima's work demonstrated a material that could exhibit unrivaled strength-to-weight ratios [3–5]. CNT fibers have exhibited exceptional mechanical performance when tested at low length scales, but when testing lengths have been increased, the observable strength decrease dramatically [6,7]. Existing testing standards point out that in manmade fibers loading conditions must be varied to accurately examine the mechanical performance. This suggests that CNT fiber studies may need to expand the testing envelop to fit industry applications if CNT fiber systems are to ever replace carbon fibers.

Continuous CNT fibers are now commercially available for scaled-up application studies [8,9], which may open the door to evently realize high-mechnical performance and engineering applications of CNT material systems. However, as a newer reinforcement material, highly systematic studies are sparce, and as such a fundamental understanding of CNTy microstrucure-

Copyright 2020. Used by the Society of the Advancement of Material and Process Engineering with permission.

property relationships at the engineering scale are underdeveloped. This study carried out scaled-up tests with large gauge lengths and morphological analysis paired with reliability statistics to reveal tensile properties, failure modes, and expectation of performance of the commercially available continuous CNT yarns in pristine and modified forms.

2. EXPERIMENTATION

2.1 Material preparation and characterization methodology

2.1.1 Raw material selection and preparation

Miralon yarns produced by Nanocomp Technologies, Inc were examined. The as received Miralon will hence forth be referred to as LCY standing for large cross-section yarn. The LCY was chemically purified at the High-Performance Materials Institute using a proprietary hot solvent process to open the LCY's dense pore structures and remove residual catalyst without causing capillary densification. Upon purification, the LCY was mechanically modified into the second yarn system used in this study – small cross-section yarns (SCY). The last yarn variant investigated was a highly densified SCY, referred to as a flattened SCY (fSCY), which was produced using a proprietary high-pressure roller device to collapse the SCY microstructure.

2.1.2 Sample structure characterization

The linear density, g/km or tex, of each yarn samples was determined by measuring the mass of a 305 mm yarn length on a Mettler Toledo XP105 analytical balance. An x-ray diffraction system was used to measure the degree of alignment of the CNTy via wide angle x-ray diffraction (WAXD). WAXD measurements were obtained on a Bruker NanoSTAR system equipped with an Incoatec IlS microfocus x-ray source. The WAXD intensity was captured by a Fuji Photo Film image plate. Each yarn type was cross-sectioned using a JEOL IB-19500CP ion beam polisher. The cross section of these samples was imaged on a Zeiss 1540EsB or JEOL 7401F field emission microscope, and yarn dimensions were measured by using area analysis in the ImageJ program.

2.1.3 Mechanical testing

To prevent out of gauge length failures, tensile samples were tested on a Shimadzu mechanical testing system equipped with a TH76-1+Ko capstan grip fixture from Grip-Engineering Thümler GmbH and 500 N load cell. The yarns were cut to 305 mm in length and tabbed to a gauge length of 100 – 120 mm with 1500 grit sandpaper tabs and Loctite 4851 adhesive. These length scales differ from most reported tests [10–12] by ~ 150 %. All samples were preloaded between 0.1 – 0.15 N, tested at a loading rate of 3 N/min, and were considered completely fractured once the measured stress dropped below 5 % of the peak stress. Load and displacement values were recorded during testing to produce the stress-strain curves. The specific stresses were calculated from the average linear density, and the strains were calculated from the elongation of the initial fiber length as measured by crosshead displacement of the mechanical testing system.

2.2 Statistical analysis procedure of mechanical results

The statistics software Minitab 19 was used for all statistical analysis. The distribution of best fit was identified from the ultimate tensile strengths for each yarn variation. Right censored parametric distribution analysis was conducted using the known failure points, and the shape, scale, and threshold parameters were determined and recorded. The distribution curves were imposed onto histograms for simplified viewing.

3. RESULTS

3.1 Microstructure characteristics of carbon nanotube yarn

3.1.1 Yarn morphology

Figure 1 shows the cross-section of the LCY, SCY, and fSCY. Notable features are the large voids present throughout the LCY and SCY samples, caused by the continuous yarn manufacturing process [13]. Aligning CNT network textiles is known to yield an increase in mechanical strength and stiffness. It is fair to suspect that the large pockets could act as defects in the LCY and SCY. Neat CNT networks rely on the van der Wahl forces and mechanical entanglement to provide homogenous load transfer [14]. Therefore, these voids would prevent CNT bundles across the gap from entangling or van der Wahl interactions. Smaller voids may exist in both LCY and SCY samples but were most likely filled due to re-deposition during cross-section preparation, which is known to happen during ion beam milling.

As the samples were modified, each yielded a different exterior surface area and morphology. From the image analysis via ImageJ, the perimeter length of each yarn variant was measured. Extrapolation using the known linear density values discussed in Section 3.1.2 of each yarn type resulted in SCY and fSCY having a 166.96 % and 363.05 % greater surface area per tex than LCY, respectively. The varying surface areas could significantly affect a polymer matrix's ability to bond to yarn and can be expected to play a critical role in interfacial strength if these yarns are to be used in future composite applications [15,16]. A circumstance of the SCY modification process was recognized in the Figure 1B – the lower portion of the SCY appears to have separated from the larger yarn mass, which indicates potential damage to the yarn surface or to the CNT bundle entanglement internally. This is could potentially exacerbate the preexisting concern of heterogeneous load transfer present from the internal voids.

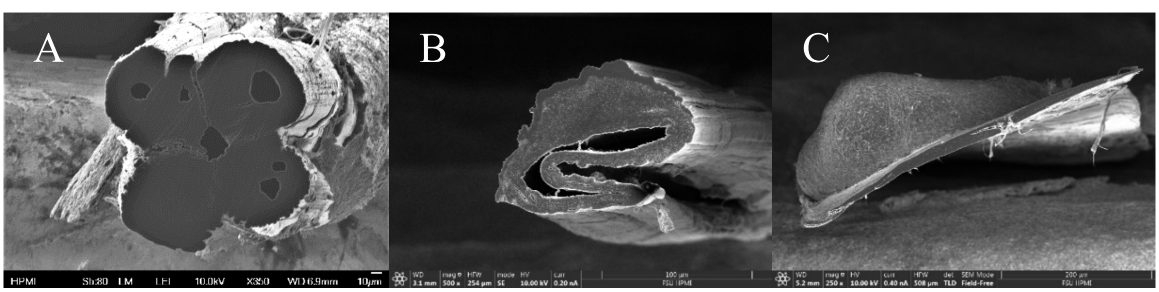

Figure 1: Scanning electron microscopy of ion beam polisher cross-sectioned LCY (A), SCY (B), and fSCY (C). The scale bars in A, B, and C are 10, 100, and 200 μm, respectively.

3.1.2 Changes in long-range order

Alignment degree plays a critical role in a CNT textile's tensile strength [17,18]. As the LCY was modified into SCY and fSCY, a concern was that the alignment degree would be negatively affected and could lead to reductions in mechanical performance during tensile tests. The associated alignment variations were characterized using the measured WAXD intensity of a crystallographic material against its crystal planes [19], and the WAXD intensity data for all three yarn types was fit to Lorentz functions. The fitted curves were procedurally applied as described in another publication [20] to Herman's orientation factor (HOF) for graphitic crystallites [21]:

$$\cos^2(\varphi) = \frac{\sum_0^{\pi/2} I(\phi) \cdot sin\,\varphi \cdot \cos^2(\phi)}{\sum_0^{\pi/2} I(\phi) \cdot sin\,\varphi} \qquad (1)$$

$$\mathrm{f} = \frac{3 \cdot \cos^2(\phi) - 1}{2} \qquad (2)$$

where $I(\phi)$ is the normalized Lorentzian fitted x-ray intensity at the respective azimuthal scan angle (ϕ).

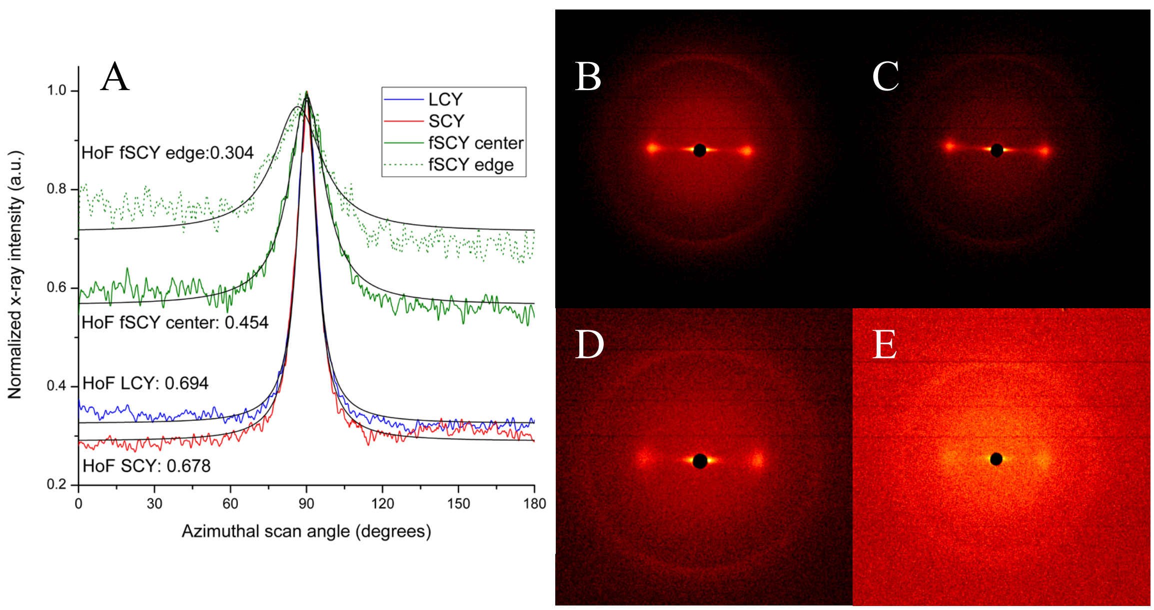

Figure 2: Combined normalized WAXD x-ray signal sets with respective fitted Lorentzian functions used in alignment analysis by Herman's orientation (A). WAXD patterns of LCY (B), SCY (C), fSCY center of yarn (D), and fSCY edge of yarn (E).

From the WAXD patterns and HOF results shown in Figure 2, the LCY and SCY exhibited similar alignment degrees at ~ 70 %, and any variations in strength or modulus were not a consequence of alignment loss from the modification process. However, fSCY was greatly affected by the densification process and exhibited a reduction of alignment across its width. From the HOF, the center of the fSCY width was calculated to be ~ 45 % aligned; however, the alignment was nonuniform across the fSCY width as the edge was ~ 30 % aligned. This noticeable drop in alignment from center to edge was determined to be a result of high compression load during the condensation process. The densification process clearly yielded increased CNT bundle packing or self-assemblage. However, it is unlikely that any benefits caused by the densification processes were unlikely to overcome the degradation of alignment.

3.2 Tensile behavior of carbon nanotube yarns

3.2.1 Capstan measurements of tensile strength

Representative specific tensile strength curves for the LCY, SCY, and fSCY are shown in Figure 5 and summarized in Table 2. The LCY exhibited the highest average specific tensile strength at 0.911 N/tex, while SCY had the highest specific stiffness at 49.634 N/tex. The SCY did not behave much differently than the LCY with the exception of a lower total strain to escape the s-tail phenomenon, discussed later in this section. The SCY specific strength on average was ~0.1 N/tex lower than LCY, while the specific stiffness increased in comparison. Interestingly, the SCY, which was expected to achieve higher specific strengths due to the improved CNT packing showed the lowest specific strength. The lack of changes in mechanical properties between LCY to SCY was minimal, so despite the reduced strength, the SCY may be better suited for composites as the modification process increased the yarn surface area, as seen in Figure 2. The fSCY performed significantly worse that the other yarns, most likely due to the previously mentioned edge defects.

The fSCY experienced the largest failure strain standard deviation, but this was expected as fSCY had a lower average degree of alignment. In cases where CNT networks were allowed to experience large deformation under loads, CNT bundles started to align, improving the mechanical properties of the CNT textile [17,22]. In fSCY samples that reached failure strains over 3 %, the stress-strain curves began to increase exponentially, agreeing with the previous CNT strain-hardening work [14,17]. As previously state, any benefits caused by densification processes were unlikely to overcome the degradation of alignment, and that CNT textiles favor network alignment compared to self-assemblage when determining mechanical performance.

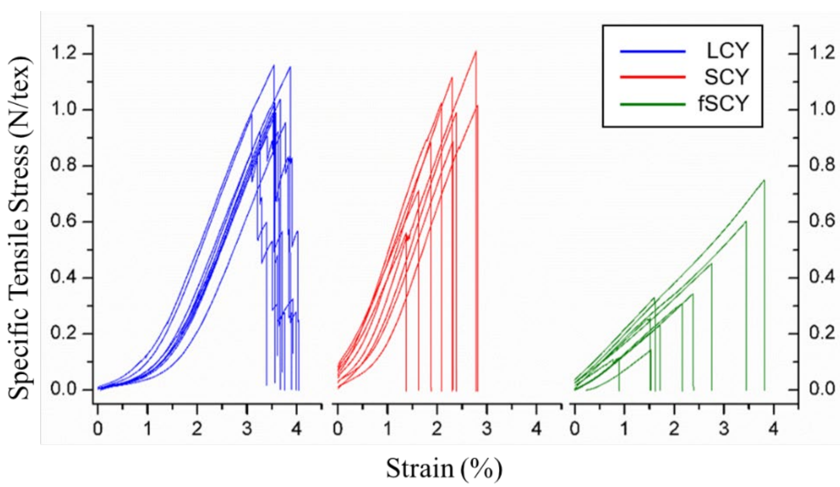

Figure 3: Specific stress-strain of random sample group of LCY, SCY, and fSCY.

Table 1: Average specific tensile properties of LCY, SCY, and fSCY.

Sample Type	Avg. Specific Tensile Strength		Avg. Specific Stiffness		Avg. Failure Strain	
	N/tex		*N/tex*		*%*	
LCY	0.911	± 0.137	46.845	± 9.778	3.186	± 0.632
SCY	0.838	± 0.211	49.634	± 7.624	2.181	± 0.542

fSCY	0.337	± 0.217	15.595	± 3.907	2.169	± 1.073

An interesting occurrence that was recorded in most samples was an s-tail at low strain percentages. This sort of behavior could be expected in tests that were started without a preload, but in extended trials, this tail was still measured in preloads as high as 1.6 % of the load at failure. This s-tail phenomenon is hypothesized to be a result of the constricting of the large pores that existed in LCY and SCY samples. From the stress-strain curves in Figure 3, this phenomenon was clearly isolated to the first ~ 1.5 % and ~ 0.5 % strains in LCY and SCY samples, respectively. This hypothesis is bolstered by the lack of the s-tail in the high density fSCY samples, which, as seen in Figure 1C, exhibited no visible pores. However, without density measurements or internal structure images of the LCY or SCY under strain, it may not be possible to confirm that the yarn pores were to blame for the stress-strain s-tail at low strains. If the yarns' loose morphology can be mitigated, the specific tensile strengths and stiffness could increase in the LCY and SCY samples.

Figure 4 graphs the specific mechanical performance of every sample, clearly showing that the densification process reduced the tensile properties while also reducing stiffness variations. Also, mechanical results showed that in their current states, the LCY, SCY, and fSCY were weaker and less stiff when compared to carbon fiber variants but similar to glass fibers available in the market.

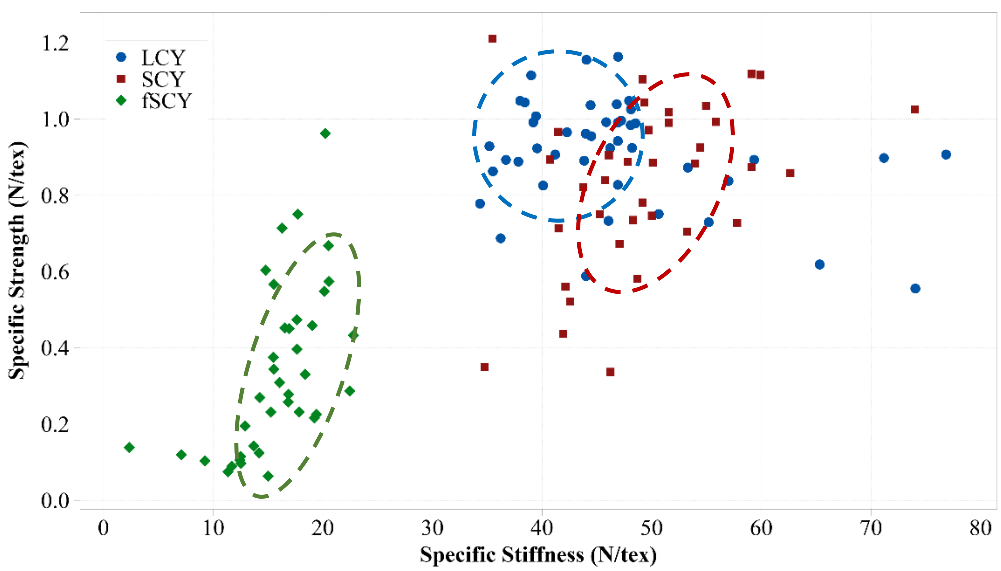

Figure 4: Specific mechanical performance distributions of tested yarn systems.

3.2.2 Fracture type categorization

Failure modes were characterized as either brittle edge or mixed mode edge. Brittle fracture was the dominant failure mode in all yarn types and can be recognized in Figure 5A,B by the distinct failure plane across the LCY and SCY. Some CNT pull out at the fracture edge was present in all brittle failures. Failure through only pullout is another unique form of failure in CNTs, higher strain or trailing force tails at failure are indicative pull out behavior. This pull-out failure is caused when the CNT network partially untangles and slides apart. Mixed mode edge failure is classified as when the failure edge shows no evident plane or exhibits multiple planes of failure and/or displayed a high degree of the pull out, as seen in Figure 5C. Figure 5D provides a simplified failure rendering to clarify how each failure typically takes shape in the yarn samples.

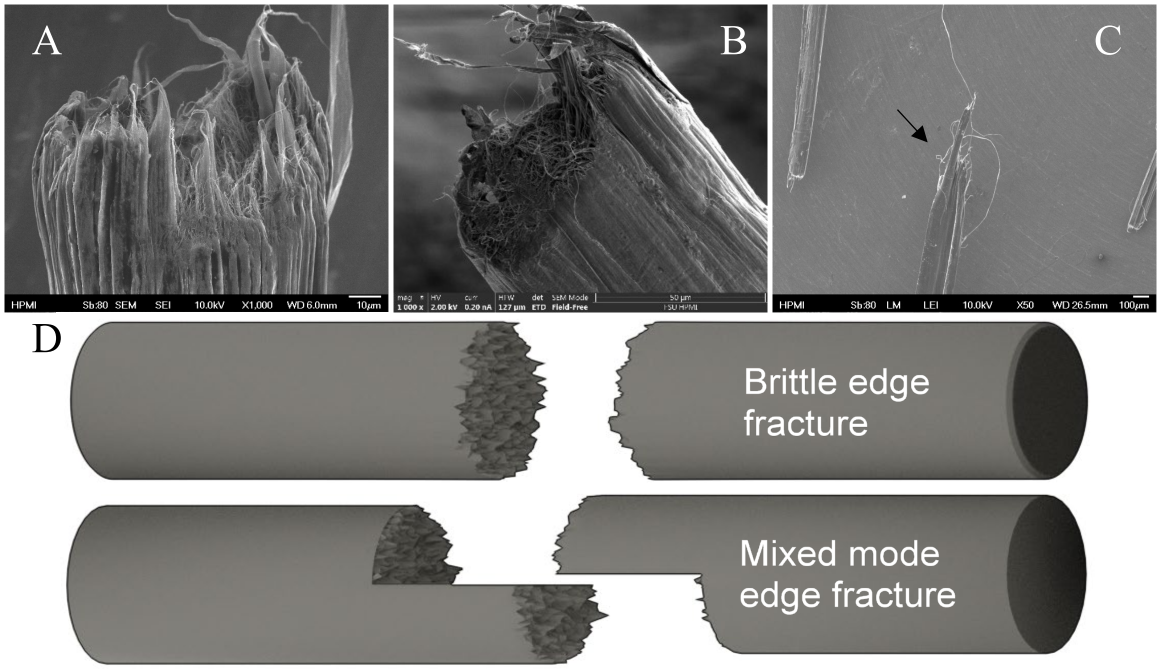

Figure 5: Brittle edge fracture of LCY quarter section (A) and SCY (B); Mixed mode edge fracture of fSCY (C); Rendering of failure modes (D).

An interesting note is that yarns which failed in brittle edge mode repetitively resulted in higher ultimate tensile strength when compared to yarns which failued by mixed mode edge. On average, the LCY, SCY, and fSCY samples that experienced brittle failures demonstrated 19.98 %, 7.89%, and 8.52 % higher ultimate tensile strengths, respectively. However, the ratio of the different failure types between yarn variants was not consistent. LCY and SCY failed in a brittle edge mode 160 % and 40 % more often than in a mixed mode edge failure, respectively; however, fCSY were 100 % more likely to fail in a mixed mode edge as opposed to a brittle edge mode. Figure 6 displays these distributions.

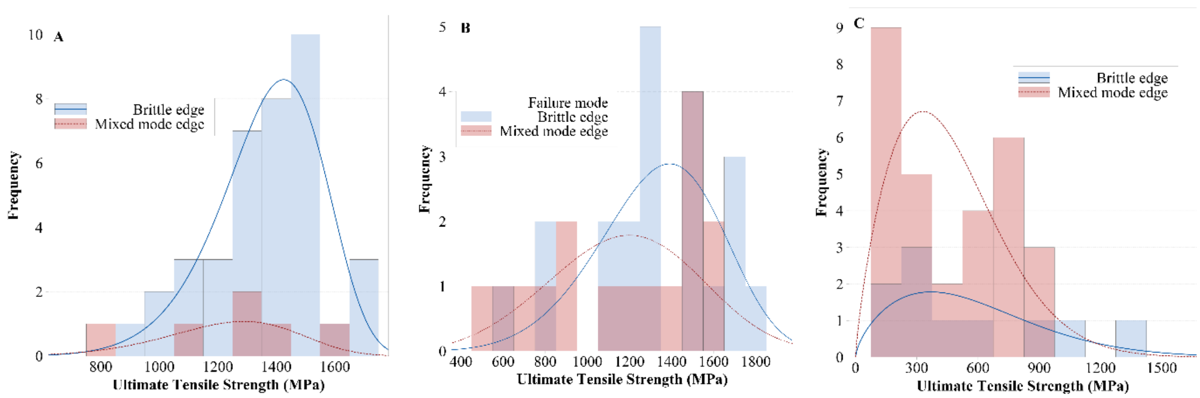

Figure 6: Histogram of ultimate tensile strength with fitted 2-parameter Weibull distribution of LCY, SCY, and fSCY grouped by brittle edge mode and mixed mode edge fractures.

Variations of CNTy surface and in-situ defects are likely the cause of the discrepancies of the different failure modes between samples. Structurally, LCY and SCY are nearly identical, apart from the yarn surfaces which differed from the mechanical modification process that SCY undergo. The high degree of edge defects that the fSCY process creates supports this claim as well. Additionally, internal impurities were recently determined to have a positive effect on mechanical properties of CNT networks in shorter length tests, while having an inverse effect as lengths increased [7]. The behavior is simplified as describing the impurities as a sort of internal sandpaper that increase friction between carbon nanotubes and their bundles. This provides support for the performance differences between the LCY or SCY and the fSCY as it is reasonable to assume that the densification process could amplify these friction effects. Moreover, this counter-effective friction behavior is likely present in the both LCY and SCY as the yarns escape the s-tail and the nonporous structure of the yarns begin to close.

3.3 Weibull analysis of tensile performance

Each specific strength data point was input into Minitab 19 to provide a probability distribution identification. Several distributions achieved excellent goodness-of-fit including smallest extreme value, 2-/3-parameter log-logistical, and 2-/3-parameter Weibull. Weibull distributions are built upon extreme value theory that serves as the basis for the weakest link model [23]. The principle driving the concept of the weakest link is that many defects compete to be the eventual site of failure. This can also provide an effective model for brittle fibers. Based on strain hardening behavior that CNT networks exhibit as their long-range alignment is increased and the abrupt failure behavior in Figure 3, the 2-parameter Weibull distribution was chosen over other distributions with similar goodness-of-fit. Furthermore, the Weibull moduli of several materials are documented, so the specific strength distributions could be easily compared.

The 2-parameter Weibull probability density function (pdf) was obtained from the pdf for a 3-parameter Weibull distribution that is displayed below:

$$f(t) = \frac{\beta}{\eta}\left(\frac{t-\gamma}{\eta}\right)^{\beta-1} e^{-\left(\frac{t-\gamma}{\eta}\right)^{\beta}} \tag{3}$$

where β is the shape parameter, η represents the scale parameter, and γ is the threshold parameter. In the 2-parameter, Weibull pdf, γ is set to zero, which in reference to this study indicates that without loading the sample cannot fail. Note that 3-parameter Weibull statistics achieved a slightly better fit than the standard 2-parameter; however, when the threshold parameter was included, it was calculated to be less than zero. This suggests that the minimum force could result in failure without any applied load; therefore, the more traditional 2-parameter Weibull was chosen to describe the failure distribution. Once the yarn distributions were chosen, the parameter probability plots were made, and the specific strengths were plotted. Figure 7 presents the statistical results. Note that β is referred to as the Weibull moduli that was used to characterize what sort of failure can be expected. For example, silicon carbide and aluminum oxide have low Weibull moduli of between 5 – 10, whereas metals like steel and aluminum range between 90 – 100 [24]. From the recorded shape parameters on the CNT yarns, the Weibull moduli closely resemble those of ceramics. The recognized Weibull shape of each yarn type agreed with previous hypothesis that the quantity and magnitude of defects are to blame for the failure in the yarns.

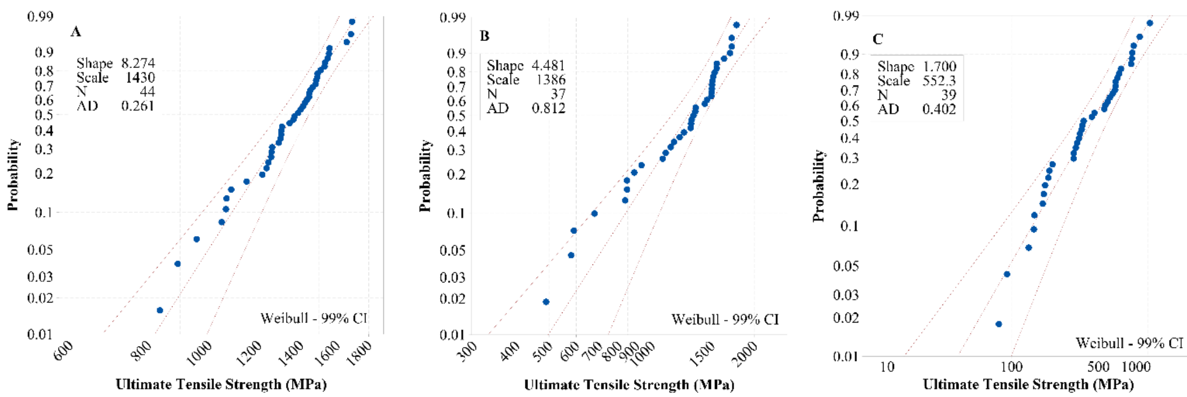

Figure 7: 99 % confidence interval 2-parameter Weibull distribution probability plot of LCY (A), SCY (B), and fSCY (C).

Despite visible micro-pull out of CNT bundles shown in Figure 1, which seem to indicate non-brittle characteristics, the Weibull distributions indicate that the failures may be driven by defects which initiate complete fractures of entangled CNTs. Consequently, at the time of failure, the van der Wahl forces holding CNTs aligned along the loading axis were unable to overcome the force suddenly applied and would slide out instantly without measurable resistance. In short, the failure of the CNT yarns as characterized under SEM appears to contain both brittle and ductile failure of the CNT network, however through Weibull distribution analysis of the ultimate tensile strength indicated that the samples failed nearly identically to materials which are traditionally viewed as brittle and showed no sign of ductile behavior.

4. CONCLUSIONS

Three variations of a commercially available CNTy were systematically studied to reveal their microstructure-mechanical property relationships and further analyzed via a combination of fracture imaging and reliability statistics. Regardless of the differing morphologies, mechanical results of the LCY and SCY show very similar performances. Self-assembly was promoted in the fSCY through mechanical densification; however, this change resulted in a reduction of alignment. Consequently, the tensile properties of fSCY were much lower than other CNTy variants. An s-tail phenomenon which was recorded in LCY and SCY samples was likely caused by the large pores, as seen in the cross-sectional SEM images. Alignment clearly is a major governing factor affecting mechanical properties, while surface defects influence how samples are expected to fail further affecting the ultimate tensile strength. Of the analyzed failure modes, the brittle edge fractures resulted in higher CNTy strength. Each data set of tensile tests was fit to an appropriate probability distribution, and the identified distribution was utilized to fit the probability density function grouped by fracture mode and probability plot for each yarn type. The experimental results for ultimate tensile strength showed a very good fit to 2-parameter Weibull statistics. The CNT yarns were concluded to exhibit brittle behavior since specific stress-strain curves showed that the CNT yarns experienced abrupt failures and the ultimate tensile strengths showed excellent fit to Weibull distributions, which is characteristic of known brittle fibers.

The experimental results show that as of now commercially available CNT yarns still exhibit lower mechanical strength and moduli compared to industrial scale production carbon fibers and other reported lab scale CNT textiles. However, a factor to consider is the lack of resin-CNT interactions that may improve load transfer throughout the CNT network. From the captured porosity images, LCY and SCY may be excellent candidates for resin infiltration; however, infiltration of fSCY may pose a challenge. These questions and observations are being addressed in on-going investigations of CNT micro-composite yarns.

5. REFERENCES

[1] Shokrieh MM, Rafiee R. A review of the mechanical properties of isolated carbon nanotubes and carbon nanotube composites. Mech Compos Mater 2010;46:155–72. https://doi.org/10.1007/s11029-010-9135-0.

[2] Al-Saleh MH, Sundararaj U. Review of the mechanical properties of carbon nanofiber/polymer composites. Compos Part A Appl Sci Manuf 2011;42:2126–42. https://doi.org/10.1016/j.compositesa.2011.08.005.

[3] Baughman RH. Carbon Nanotubes--the Route Toward Applications. Science (80-) 2002;297:787–92. https://doi.org/10.1126/science.1060928.

[4] Bai Y, Zhang R, Ye X, Zhu Z, Xie H, Shen B, et al. Carbon nanotube bundles with tensile strength over 80 GPa. Nat Nanotechnol 2018;13:589–95. https://doi.org/10.1038/s41565-018-0141-z.

[5] Ding H, Zhang Q, Wang F, Tian Y, Wang L, Shi Y, et al. Structure control of polyphenylene sulfide membrane prepared by thermally induced phase separation. J Appl Polym Sci 2007;105:3280–6. https://doi.org/10.1002/app.26595.

[6] Koziol K, Vilatela J, Moisala A, Motta M, Cunniff P, Sennett M, et al. High-Performance Carbon Nanotube Fiber. Science (80-) 2007;318:1892–5. https://doi.org/10.1126/science.1147635.

[7] Gspann TS, Montinaro N, Pantano A, Elliott JA, Windle AH. Mechanical properties of carbon nanotube fibres: St Venant's principle at the limit and the role of imperfections. Carbon N Y 2015;93:1021–33. https://doi.org/10.1016/j.carbon.2015.05.065.

[8] Siochi EJ, Harrison JS. Structural nanocomposites for aerospace applications. MRS Bull 2015;40:829–35. https://doi.org/10.1557/mrs.2015.228.

[9] Kim J-W, Sauti G, Wincheski RA, Cano RJ, Jensen BD, Smith Jr. JG, et al. Undirectional Carbon Nanotube Yarn/Polymer Composites. Hampton, Virginia: 2018.

[10] Evora MC, Lu X, Hiremath N, Kang N-G, Hong K, Uribe R, et al. Single-step process to improve the mechanical properties of carbon nanotube yarn. Beilstein J Nanotechnol 2018;9:545–54. https://doi.org/10.3762/bjnano.9.52.

[11] Humble J. Modeling of nonisothermal crystallization kinetics of semilinear polyphenylene sulfide for process simulation. Annu Tech Conf - ANTEC, Conf Proc 2016:632–8.

[12] Sugano K, Kurata M, Kawada H. Evaluation of mechanical properties of untwisted carbon nanotube yarn for application to composite materials. Carbon N Y 2014;78:356–65. https://doi.org/10.1016/j.carbon.2014.07.012.

[13] Lashmore DS, Braden R, Hart AJ, Welch J. Chemically-assisted alignment of nanotubes within extensible structures. US 8,246,886 B2, 2012.

[14] Downes RD, Hao A, Park JG, Su Y-F, Liang R, Jensen BD, et al. Geometrically constrained self-assembly and crystal packing of flattened and aligned carbon nanotubes. Carbon N Y 2015;93:953–66. https://doi.org/10.1016/j.carbon.2015.06.012.

[15] Peng Q, He X, Li Y, Wang C, Wang R, Hu P, et al. Chemically and uniformly grafting carbon nanotubes onto carbon fibers by poly(amidoamine) for enhancing interfacial strength in carbon fiber composites. J Mater Chem 2012;22:5928. https://doi.org/10.1039/c2jm16723a.

[16] Xiao T, Liu J, Xiong H. Effects of different functionalization schemes on the interfacial strength of carbon nanotube polyethylene composite. Acta Mech Solida Sin 2015;28:277–84. https://doi.org/10.1016/S0894-9166(15)30014-8.

[17] Jolowsky C, Sweat R, Park JG, Hao A, Liang R. Microstructure evolution and self-assembling of CNT networks during mechanical stretching and mechanical properties of highly aligned CNT composites. Compos Sci Technol 2018;166:125–30. https://doi.org/10.1016/j.compscitech.2018.04.003.

[18] Ma W, Liu L, Zhang Z, Yang R, Liu G, Zhang T, et al. High-Strength Composite Fibers: Realizing True Potential of Carbon Nanotubes in Polymer Matrix through Continuous Reticulate Architecture and Molecular Level Couplings. Nano Lett 2009;9:2855–61. https://doi.org/10.1021/nl901035v.

[19] White JL, Spruiell JE. The specification of orientation and its development in polymer processing. Polym Eng Sci 1983;23:247–56. https://doi.org/10.1002/pen.760230503.

[20] Moharir AV, Vijayraghavan KM, Panda BC, Gupta VB. Dependence of Stiffness and Strength of Cotton Fibers on Crystallite Orientation. Text Res J 1982;52:756–60.

https://doi.org/10.1177/004051758205201204.

[21] Hermans PH, Weidinger A. Quantitative X-Ray Investigations on the Crystallinity of Cellulose Fibers. A Background Analysis. J Appl Phys 1948;19:491–506. https://doi.org/10.1063/1.1698162.

[22] Downes R, Wang S, Haldane D, Moench A, Liang R. Strain-Induced Alignment Mechanisms of Carbon Nanotube Networks. Adv Eng Mater 2015;17:349–58. https://doi.org/10.1002/adem.201400045.

[23] Zok FW. On weakest link theory and Weibull statistics. J Am Ceram Soc 2017;100:1265–8. https://doi.org/10.1111/jace.14665.

[24] Meyers MA, Chawla KK. Statistical Analysis of Failure Strength. Mech. Behav. Mater. 2nd ed., New York City, NY: Cambridge University Press; 2009, p. 449–60.